Proceedings of the Combustion Institute 40 (2024) 105537

Contents lists available at ScienceDirect

Proceedings of the Combustion Institute

journal homepage: www.elsevier.com/locate/proci

Scalar mass conservation in LES of soot formation using mixture fraction-based combustion models

Marco Davidovic *, Heinz Pitsch

Institute for Combustion Technology, RWTH Aachen University, Aachen 52056, Germany

ARTICLE INFO

Keywords:
Flamelet
LES
Non-premixed
Soot
Scalar mass conservation

ABSTRACT

Mixture fraction-based models, such as non-premixed flamelet or Conditional Moment Closure (CMC) models, find widespread application in the investigation of turbulent combustion and pollutant formation. These models solve for the mixing field in physical space, while the chemistry solution is obtained in mixture fraction space. The coupling between the two fields is accomplished by two flow-dependent parameters governing the transport in mixture fraction space. These parameters must be computed consistently with the mixture fraction field evolution in order to preserve scalar mass conservation. Analytic expressions can be derived for obtaining these flow parameters consistently to the widely applied presumed Filtered Density Function (FDF) approach. Two approaches are considered in this paper: the local model formulates the local flow parameters consistently with the local FDF evolution before determining the global flow parameters through volume averaging. The global model integrates the FDF in physical space first and then determines the global flow parameter directly from the global mixture distribution evolution. These two models are employed in Large Eddy Simulations (LES) of an auto-igniting *n*-dodecane spray. The simulation results are compared with each other and to a conventional flow parameters model, with a specific focus on scalar mass conservation. Both new models outperform the conventional model in terms of scalar mass conservation, with the most pronounced effect observed for soot. Furthermore, it is demonstrated that, although both new models are analytically equal, numerical errors arising from scalar convection terms in the LES solver impact mass conservation properties differently. The local model accurately predicts conditional flow parameters but suffers from numerical inconsistencies within discretized equations, resulting in scalar mass conservation errors, particularly for highly-diffusive numerical schemes. In contrast, the global model incorporates numerical errors from the flow solver within the flow parameters, thus yielding small conservation errors for all considered scalar convection schemes.

1. Introduction

Non-premixed turbulent combustion plays a pivotal role in various technical applications, such as internal combustion engines and gas turbines, serving as a significant contributor to current energy demands. However, this widespread utilization also leads to substantial global warming and environmental pollution. In an effort to mitigate these issues, there is a growing focus on replacing traditional fossil fuels with alternative liquid fuels synthesized from renewable energy sources and carbon feedstocks. While this transition can reduce net greenhouse gas emissions, challenges persist in minimizing the production of harmful pollutants like nitrogen oxides (NO_x) and particulate matter (PM).

Despite considerable research efforts spanning several decades, accurately predicting pollutant formation during combustion remains a complex task. The intricacy of the problem arises from the multi-physics interactions occurring over a wide range of length and time scales. In addressing this complexity, modern research has adopted Large-Eddy Simulations (LES) employing detailed chemistry combustion models. Among these, mixture fraction-based approaches, such as flamelet and conditional moment closure (CMC) models, have emerged as popular choices. This preference is attributed to their computational efficiency, making them particularly well-suited for modeling non-premixed combustion in turbulent flames.

Mixture fraction-based combustion models decompose the evolution of reactive scalars into the transport of mixture fraction, Z, in physical space and the evolution of scalars relative to mixture fraction. Central to these models are the conditional flow parameters: scalar dissipation rate, $\overline{\chi_Z|\psi}$, and diffusion rate, $\overline{\xi_Z|\psi}$, which govern the transport in mixture fraction space and are defined as

$$\overline{\chi_Z|\psi} = \overline{2D\frac{\partial Z}{\partial x_i}\frac{\partial Z}{\partial x_i}\Big|\psi}, \tag{1}$$

* Corresponding author.
E-mail address: m.davidovic@itv.rwth-aachen.de (M. Davidovic).

https://doi.org/10.1016/j.proci.2024.105537
Received 4 December 2023; Accepted 29 June 2024
Available online 24 July 2024

$$\overline{\xi_Z|\psi} = \overline{\frac{1}{\rho}\frac{\partial}{\partial x_i}\left(\rho D\frac{\partial Z}{\partial x_i}\right)\Bigg|\psi}, \tag{2}$$

where x_i are the spatial coordinates, D is the mixture fraction diffusivity, ρ is the density, and ψ is the mixture fraction sample space variable. Although the flow parameters are often chosen independently for simplicity, it is necessary to formulate them consistently with the mixture fraction field evolution to ensure conservative scalar mixing [1,2]. The significance of this consistency is particularly pronounced in mixture fraction-based soot modeling, where conventional flow parameter models can introduce conservation errors of leading order [2].

The mixing field evolution is coupled to the conditional flow parameters through the Filtered Density Function (FDF) transport equation, which can be derived following the procedure described by Pope [3] and is - in the absence of mixture fraction sources - given by

$$\frac{\partial\overline{\rho}\widetilde{f}_Z}{\partial t} + \frac{\partial\overline{\rho}\,\overline{u_i|\psi}\,\widetilde{f}_Z}{\partial x_i} = -\frac{\partial\overline{\rho}\widetilde{f}_Z\,\overline{\xi_Z|\psi}}{\partial\psi} = \frac{\partial}{\partial x_i}\left(\overline{\rho D\frac{\partial f'_Z}{\partial x_i}}\right) - \frac{1}{2}\frac{\partial^2\overline{\rho}\widetilde{f}_Z\,\overline{\chi_Z|\psi}}{\partial\psi^2}, \tag{3}$$

where t denotes the time, u_i the velocity components, $\widetilde{f}_Z$ the Favre FDF, and f'_Z the fine-grained FDF.

In principle, two approaches can be followed. The conditional parameters can be modeled, e.g., by presuming a functional form that is scaled such that its unconditional filtered value is recovered, and the mixing field evolution is then obtained accordingly by solving Eq. (3). This approach has been proposed by Ilgun, Passalacqua, and Fox [4,5]. In the second approach, the mixture fraction FDF evolution is modeled in a simplified manner, and the conditional flow parameters are determined accordingly. A common approach to model the FDF evolution is the presumed FDF method, which presumes a functional form for the FDF that is parameterized by low-order mixture fraction moments. Modeled equations are then solved for these moments in physical space. Recently, Davidovic and Pitsch [6] derived a formulation to express the conditional flow parameters consistently with the beta distribution. The flow parameter model has been applied to the inert ECN Spray A case, and the model predictions have been compared to a conventional model. These results indicated that conventional models can suffer from strong conservation errors, particularly for non-unity Lewis number scalars. This hypothesis is addressed in the current work, where the revised model is applied to a reactive spray case. The scalar mass conservation properties of the revised model are compared to a conventional model for both unity and non-unity Lewis number scalars.

The revised model is analytically consistent and, therefore, prevents scalar mass conservation errors when solved accurately. However, as in the present study, LES of turbulent combustion typically employ spatial discretization, such as finite differences, and is commonly based on implicit filtering, which has been shown to be susceptible to both aliasing and truncation errors [7–9]. Note that in this paper, the terminology scalar mass conservation refers to the conservation property of the transport scheme, excluding chemical source terms. While the effect of numerical errors in LES on the filtered flow field has been extensively studied, the propagation of these errors for state-space combustion models has not yet been discussed. Thus, the objective of this paper is twofold. In addition to evaluating the importance of consistent flow parameter modeling under engine-relevant conditions, we investigate the propagation of numerical errors arising from the flow solver into the prediction of the mixture fraction-based combustion model. In other words, this study focuses on the scalar mass conservation properties of the numerical schemes rather than comparing the simulation results to experimental data.

The structure of the paper unfolds as follows: Section 2 briefly summarizes the required theoretical background and presents the two formulations of the consistent conditional flow parameter model. The models are then applied to a single-hole *n*-dodecane injection case. The case and the results are presented in Section 3. The paper closes with a summary and conclusions in Section 4.

2. Theory

The relevant theoretical background is provided in this section. Firstly, the unsteady, non-premixed global flamelet equations are described. Subsequently, three different flow parameter models, applied later in this paper, are presented and discussed. These flow parameter models address numerical errors originating from the flow solver in different ways. A theoretical discussion is presented at the end of this section.

2.1. Non-premixed flamelet equation

In the absence of liquid spray droplets, the spatial and temporal evolution of a Favre-filtered reactive scalar, $\widetilde{\phi}$, is given by

$$\frac{\partial\overline{\rho}\widetilde{\phi}}{\partial t} + \frac{\partial\overline{\rho u_i}\widetilde{\phi}}{\partial x_i} = \frac{1}{\mathrm{Le}_\phi}\frac{\partial}{\partial x_i}\left(\overline{\rho D\frac{\partial\phi}{\partial x_i}}\right) + \overline{\dot{\omega}}_\phi, \tag{4}$$

where ϕ can represent species mass fractions, temperature, or mass-related soot scalars and $\overline{\dot{\omega}}_\phi$ denotes the corresponding chemical source term. Le_ϕ is the scalar Lewis number that is assumed to be constant. Using the flamelet assumption, Eq. (4) can be transformed into mixture fraction space. The resulting global flamelet equations reads

$$\frac{\partial\hat{\phi}}{\partial t} + \xi_G\left(1 - \frac{1}{\mathrm{Le}_\phi}\right)\frac{\partial\hat{\phi}}{\partial\psi} = \frac{\chi_G}{2\mathrm{Le}_\phi}\frac{\partial^2\hat{\phi}}{\partial\psi^2} + \frac{\hat{\dot{\omega}}_\phi}{\hat{\rho}}, \tag{5}$$

where the hat symbol denotes quantities in mixture fraction space. χ_G and ξ_G are the global conditional mixture fraction dissipation and diffusion rate, respectively, which are defined as

$$\chi_G = \frac{\int\overline{\rho}\widetilde{f}_Z\,\overline{\chi_Z|\psi}\,\mathrm{d}V}{\int\overline{\rho}\widetilde{f}_Z\mathrm{d}V}, \tag{6}$$

$$\xi_G = \frac{\int\overline{\rho}\widetilde{f}_Z\,\overline{\xi_Z|\psi}\,\mathrm{d}V}{\int\overline{\rho}\widetilde{f}_Z\mathrm{d}V}. \tag{7}$$

Note that Triantalyllidis and Mastorakos [10] have also proposed Eq. (6) and Eq. (7) for calculating volume-averaged conditional flow parameters in CMC-LES models.

It can be seen in Eq. (5) that χ_G acts as diffusivity and ξ_G as convective velocity in mixture fraction space. For more details on the flamelet equation derivation, the reader is referred to our prior work [6].

The local filtered scalar value is reconstructed using the flamelet solution and the local FDF according to

$$\widetilde{\phi} = \int_0^1 \widetilde{f}_Z\hat{\phi}\,\mathrm{d}\psi. \tag{8}$$

Note that $\widetilde{f}_Z$ depends on space, x_i, time, t, and sample space, ψ, i.e., $\widetilde{f}_Z = f(x_i, t; \psi)$. However, the functional dependency is dropped for the sake of readability. Also, note that the modified beta distribution, which has been proposed by Ge and Gutheil [11] for turbulent sprays, is employed as FDF within this study.

2.2. Conditional flow parameter models

Three different models are employed in this study, and they are compared concerning their scalar mass conservation capabilities. The first model is a conventional one widely used in the literature, which does not maintain consistency with the FDF evolution. The other two models are formulated consistently with the FDF evolution but differ in terms of computational efficiency and applicability.

2.2.1. Inverse Error Function (ERFC) model

The widely applied scalar dissipation rate model derived by Peters [12], which closely approximates the scalar dissipation rate profile of a counterflow diffusion flame, is used as a reference model in this study. In this model, the scalar dissipation rate is approximated using an inverse complementary error function profile given by

$$\overline{\chi_Z|\psi} = \chi_{\mathrm{ref}} \exp\left(2\left[\mathrm{erfc}^{-1}(2Z_{\mathrm{ref}})\right]^2 - 2\left[\mathrm{erfc}^{-1}(2Z)\right]^2\right). \tag{9}$$

The reference scalar dissipation rate, χ_{ref}, is obtained such that the unconditionally filtered scalar dissipation rate $\widetilde{\chi}_Z$ is recovered given the local FDF ($\widetilde{\chi}_Z = \int_0^1 \widetilde{f}_Z \overline{\chi_Z|\psi}\,\mathrm{d}\psi$). When curvature effects are neglected, the conditional diffusion rate can be expressed by the scalar dissipation rate profile [13] and is given by

$$\overline{\xi_Z|\psi} = \frac{1}{4\hat{\rho}}\left[\frac{\partial \hat{\rho}\,\overline{\chi_Z|\psi}}{\partial\psi} + \frac{\overline{\chi_Z|\psi}}{\hat{D}}\frac{\partial \hat{\rho}\hat{D}}{\partial\psi}\right]. \tag{10}$$

Note that the flow parameters are obtained independently of the FDF evolution in this model, and hence, using this model in combination with a presumed FDF approach may result in scalar mass conservation errors.

2.2.2. Global Consistent Flow Parameters (GCFP) model

The GCFP model expresses global flow parameters consistently with the global FDF evolution, irrespective of the specific model employed to derive the global FDF. The model's principal aim is the direct computation of global conditional flow parameters from the global mixture evolution without explicit calculation of local parameters $\overline{\chi_Z|\psi}$ and $\overline{\xi_Z|\psi}$. This methodology, however, necessitates additional model assumptions, specifically, a closed system and the absence of mixture fraction or mass source terms due to evaporation. If evaporation source terms are present, a conditional source term appears in Eq. (3), which needs to be formulated consistently with the filtered evaporation source terms in the mixture fraction moments equations. A mathematical formulation has been derived in our prior work [6]. However, it was shown that the beta distribution is not able to preserve the physical constraints of the evaporation model. Invoking the aforementioned assumptions, Eq. (3) can be integrated over the entire system volume, effectively eliminating convection and diffusion terms. The resulting global flow parameters are obtained through integration in mixture fraction space, as expressed by

$$\chi_G = -\frac{2}{\widetilde{f}_G}\int_0^{\psi}\frac{\partial \widetilde{f}_G}{\partial t}\mathrm{d}\psi'\mathrm{d}\psi', \tag{11}$$

$$\xi_G = -\frac{1}{\widetilde{f}_G}\int_0^{\psi}\frac{\partial \widetilde{f}_G}{\partial t}\mathrm{d}\psi', \tag{12}$$

where $\widetilde{f}_G$ is the global mixture distribution function, which is defined as $\widetilde{f}_G = \int \overline{\rho}\widetilde{f}_Z \mathrm{d}V$. The numerical evaluation of Eqs. (11) and (12) appears straightforward, as only the temporal evolution of the global FDF has to be provided by the flow solver, which can be approximated from multiple FDF fields at different time-instances using finite differences. However, the evaluation of the GCFP model can be sensitive to numerical errors arising from the numerical integration in mixture fraction space, particularly at mixture fraction locations where $\widetilde{f}_G$ is small. Yet, if the mixture fraction grid is sufficiently fine, the numerical evaluation of Eqs. (11) and (12) provided good results in a previous study [2]. Additionally, due to the imposed model assumptions, the GCFP model has a limited applicability and cannot be employed in flows involving fuel evaporation.

2.2.3. Local Consistent Flow Parameters (LCFP) model

In contrast to the GCFP model, the LCFP approach seeks to initially compute the local conditional flow parameters ($\overline{\chi_Z|\psi}$ and $\overline{\xi_Z|\psi}$), followed by the evaluation of global conditional flow parameters through Eqs. (6) and (7). The local flow parameters can be determined by expressing the left-hand side of Eq. (3) through the presumed functional dependency of $\widetilde{f}_Z$ on the mixture fraction moments and the modeled evolution of those moments. If the FDF is parameterized by the first two mixture fraction moments, the local conditional flow parameters are given by

$$\widetilde{f}_Z\,\overline{\chi_Z|\psi} = 2\widetilde{\chi}_Z\frac{\partial \widetilde{\mathbf{F}}_Z}{\partial \widetilde{Z^2}} + \widetilde{\chi}_{\widetilde{Z}\widetilde{Z}}\frac{\partial^2 \widetilde{\mathbf{F}}_Z}{\partial \widetilde{Z}^2} + 2\widetilde{\chi}_{\widetilde{Z}\widetilde{Z^2}}\frac{\partial^2 \widetilde{\mathbf{F}}_Z}{\partial \widetilde{Z}\partial \widetilde{Z^2}} + \widetilde{\chi}_{\widetilde{Z^2}\widetilde{Z^2}}\frac{\partial^2 \widetilde{\mathbf{F}}_Z}{\partial \widetilde{Z^2}^2}, \tag{13}$$

and

$$\begin{aligned}\widetilde{f}_Z\,\overline{\xi_Z|\psi} = &-\xi_{\widetilde{Z}}\frac{\partial \widetilde{F}_Z}{\partial \widetilde{Z}} - \left(\xi_{\widetilde{Z^2}} - \widetilde{\chi}_Z\right)\frac{\partial \widetilde{F}_Z}{\partial \widetilde{Z^2}} \\ &+ \frac{\widetilde{\chi}_{\widetilde{Z}\widetilde{Z},t}}{2}\frac{\partial^2 \widetilde{F}_Z}{\partial \widetilde{Z}^2} + \widetilde{\chi}_{\widetilde{Z}\widetilde{Z^2},t}\frac{\partial^2 \widetilde{F}_Z}{\partial \widetilde{Z}\,\widetilde{Z^2}} + \frac{\widetilde{\chi}_{\widetilde{Z^2}\widetilde{Z^2},t}}{2}\frac{\partial^2 \widetilde{F}_Z}{\partial \widetilde{Z^2}^2},\end{aligned} \tag{14}$$

where new variables have been introduced for better readability, which are defined as

$$\widetilde{F}_Z = \int_{-\infty}^{\psi}\widetilde{f}_Z\left(\psi';\widetilde{Z},\widetilde{Z^2}\right)\mathrm{d}\psi', \tag{15}$$

$$\widetilde{\mathbf{F}}_Z = \iint_{-\infty}^{\psi}\widetilde{f}_Z\left(\psi';\widetilde{Z},\widetilde{Z^2}\right)\mathrm{d}\psi'\mathrm{d}\psi', \tag{16}$$

$$\widetilde{\chi}_{\alpha\beta} = 2\left(\widetilde{D} + \widetilde{D}_t\right)\frac{\partial\alpha}{\partial x_i}\frac{\partial\beta}{\partial x_i}, \tag{17}$$

$$\widetilde{\chi}_{\alpha\beta,t} = 2\widetilde{D}_t\frac{\partial\alpha}{\partial x_i}\frac{\partial\beta}{\partial x_i}, \tag{18}$$

$$\xi_\alpha = \frac{1}{\overline{\rho}}\frac{\partial}{\partial x_i}\left(\overline{\rho}\widetilde{D}\frac{\partial\alpha}{\partial x_i}\right), \tag{19}$$

where α and β are placeholders for combinations of $\widetilde{Z}$ and $\widetilde{Z^2}$.

Note that Eq. (15) and Eq. (16) can be integrated analytically when a beta distribution is employed as FDF. Consequently, in contrast to the GCFP model, the LCFP model is not susceptible to discretization errors arising from the mixture fraction grid. In principle, an analytical evaluation of the partial derivatives of $\widetilde{F}_Z$ and $\widetilde{\mathbf{F}}_Z$ with respect to $\widetilde{Z}$ and $\widetilde{Z^2}$ in Eq. (13) and Eq. (14) is also possible. However, these expressions become unwieldy and computationally expensive. Thus, the partial derivatives are numerically evaluated using central differences. Furthermore, the LCFP model can be applied to open systems or flows with evaporating fuel. For more details on the derivation of the LCFP model, the reader is referred to our prior work [6].

2.3. Assessment and propagation of numerical errors

LES of turbulent flows are prone to numerical errors, primarily stemming from the discretization of the non-linear convective term [8]. Those errors manifest in the FDF field through the transport of $\widetilde{Z}$ and $\widetilde{Z^2}$. Consequently, even if the transport of $\hat{\phi}$ in mixture fraction space is solved accurately, a scalar mass conservation error might appear in physical space through the combination of $\widetilde{f}_Z$ and $\hat{\phi}$ in Eq. (8). To evaluate those conservation errors, Eq. (4) is integrated over the entire system volume. Assuming a closed system and invoking Eq. (8) yields

$$\frac{\mathrm{d}\boldsymbol{\Phi}}{\mathrm{d}t} = \int_V \overline{\rho}\int_0^1 \widetilde{f}_Z\frac{\dot{\hat{\omega}}_\phi}{\hat{\rho}}\mathrm{d}\psi\mathrm{d}V, \tag{20}$$

with $\boldsymbol{\Phi} = \int_V \overline{\rho}\int_0^1 \widetilde{f}_Z\hat{\phi}\mathrm{d}\psi\mathrm{d}V$. Thus, Eq. (20) can be used to evaluate the evolution of the total scalar mass isolated from conservation errors due to transport modeling inconsistencies or numerical errors arising from transport terms. Thus, the accumulated scalar mass conservation error, ϵ_ϕ, can be estimated at each time step using the solution from Eq. (20) and the filtered scalar field computed via Eq. (8) according to

$$\epsilon_\phi = \left|\int_{t_0}^{t}\frac{\mathrm{d}\boldsymbol{\Phi}}{\mathrm{d}t}\mathrm{d}t - \left[\int_V \overline{\rho}\widetilde{\phi}\mathrm{d}V - \boldsymbol{\Phi}_0\right]\right|, \tag{21}$$

where $\boldsymbol{\Phi}_0$ is the total scalar mass at $t = t_0$.

It is noteworthy that in a closed system without fuel evaporation, the GCFP and LCFP models are mathematically identical and should yield equivalent results if solved accurately. The LCFP model, requiring only an instantaneous flow field for evaluation, ensures that the predicted flow parameters remain uncontaminated by numerical errors associated with the convective term. In contrast, the GCFP model relies on the temporal evolution of the global mixture distribution function, which is governed by the transport of $\widetilde{Z}$ and $\widetilde{Z^2}$. Consequently, the temporal evolution observed by the GCFP model is influenced by numerical errors arising from the convective transport of $\widetilde{Z}$ and $\widetilde{Z^2}$. This leads to the prediction of flow parameters by the GCFP model being impacted by the numerical scheme employed for convective scalar fluxes.

3. Model application

The different flow parameter models are applied in reactive spray LES in this section. Firstly, the simulation case and setup are briefly described. Afterwards, the numerical methods and models used in this work are summarized. Lastly, the simulation results are presented and discussed.

3.1. Simulation case and setup

A single-hole, high-pressure, *n*-dodecane injection is studied in this work, which corresponds to the well-known ECN Spray A case. However, to be able to focus on the mathematical formulation and its interaction with numerical errors, a single-flamelet model is employed. This does not capture variations in conditional reaction progress. Hence, the injection duration has been artificially shortened to 0.4 ms. The ambient gas has a temperature of 900 K at a pressure of 60 bar and an oxygen mole fraction of 15 %. The injection rate corresponds to 1500 bar injection pressure.

The flow solver grid has a minimum grid spacing of 100 μm at the nozzle orifice and corresponds to a grid used in a previous study [6]. However, since a shortened injection duration is considered, the grid dimensions have been reduced.

3.2. Numerical simulation framework

A fully compressible solver is employed for the gas phase, while the dispersed liquid phase is solved in a Lagrangian formulation. The conservation of energy is solved using the internal energy formulation, while the ideal gas law is employed as equation of state. The unresolved Reynolds stresses and scalar fluxes are modeled using a dynamic Smagorinsky model (DSM) [14]. Note that the coherent structures subfilter model (CSM) by Kobayashi [15] has also been tested and yields similar results in terms of scalar mass conservation. The subfilter model comparison is provided in the supporting material. Mass, momentum, and energy transfer with the dispersed phase are calculated using state-of-the-art drag and evaporation models [16]. A Rosin-Rammler distribution is used for the initial droplet size distribution, while secondary breakup is modeled using the Kelvin–Helmholtz Rayleigh–Taylor model [17]. For more details on the spray LES model, the reader is referred to our prior work [6].

Unsteady non-premixed flamelet equations, Eq. (5), are solved interactively with the flow for all species, temperature, and soot scalars [18]. Following Attili et al. [19], unity Lewis numbers are used for all species representing the role of turbulent transport. Hence, the species transport in mixture fraction space is independent of ξ_G. A reduced chemical mechanism is employed for the *n*-dodecane chemistry [20]. The formation of polycyclic aromatic hydrocarbons (PAH) is modeled based on the mechanism of Narayanaswamy et al. [21]. The HMOM soot model [22], which uses a bivariate description of soot particles and is based on detailed PAH chemistry, is employed for predicting the soot evolution. Soot particle diffusion and thermophoretic transport are neglected. Thus, the flamelet equation is solved in the $Le_\phi \to \infty$ limit for all soot moments, which makes the soot transport in mixture fraction space independent of χ_G.

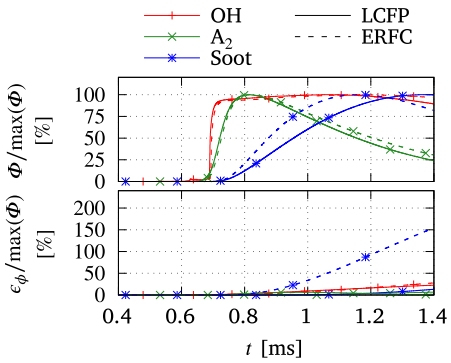

Fig. 1. Normalized scalar mass (top) and scalar mass conservation error (bottom) for OH, naphthalene (A_2), and soot for the LCFP and ERFC model in the full injection case.

All simulations were performed using the in-house flow solver CIAO. The filtered Navier–Stokes equations are solved on a structured staggered Cartesian grid. A scalar convection scheme variation is performed, including conservative central differences [23], QUICK [24], BQUICK [25], and WENO schemes [26] of different order. Other terms are spatially discretized using conservative central differences of 2nd order [23]. The time integration is performed using an explicit low-storage five-stage Runge–Kutta (RK) method with 2nd order accuracy [27,28]. The flow time step is limited by an acoustic Courant–Friedrichs–Lewy (CFL) condition enforcing CFL numbers below 1. The Lagrangian particles are advanced using a 2nd order RK method that employs adaptive time-stepping. The flamelet equations are discretized using 2nd order central differences for the diffusive term and 1st order upwind for the convective term, while the CVODE solver [29] has been used for time-integration of the flamelet equation.

3.3. Results

Full injection cases have been performed for the ERFC and the LCFP model. The flamelet grid has been discretized using 192 grid points, and WENO5 has been used to approximate the convective scalar fluxes.

The total scalar mass and conservation errors, as defined by Eq. (21), are depicted for OH, naphthalene A_2, and soot in the top and bottom plots of Fig. 1, respectively. Note that both the scalar mass and the conservation error are normalized by the corresponding maximum scalar mass. The selection of A_2 and OH is motivated by their pivotal roles in soot formation and soot oxidation. Notably, the LCFP and ERFC models exhibit similar predictions for OH and A_2, while there is a substantial deviation in the predicted soot mass. The bottom plot in Fig. 1 reveals that this difference primarily originates from conservation errors arising due to inconsistent soot transport. Concurrently, despite the LCFP model improving scalar mass conservation in comparison to the conventional ERFC model, a non-negligible conservation error persists. Given the analytical consistency of the LCFP equations with the FDF transport equation, the remaining scalar mass conservation issue must be attributed to numerical errors.

Note that a grid variation study has been performed, showing that scalar mass conservation errors are also significant at refined grid spacings. The results of this grid study are provided within the supporting material.

Since numerical errors in LES are commonly dominated by the convective flux discretization, further simulations have been conducted to study the effect of the scalar convection scheme on the conservation properties of the different models. The configuration has been tailored such that other sources of errors are small. The flow field of the full

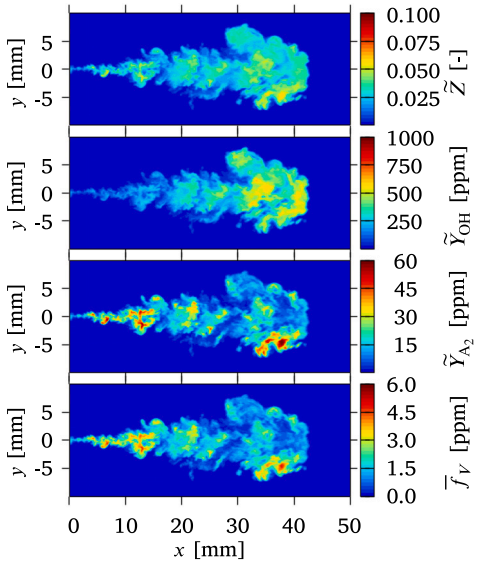

Fig. 2. Initial solutions for the filtered mixture fraction, $\widetilde{Z}$, filtered OH mass fraction, $\widetilde{Y}_{OH}$, filtered naphthalene mass fraction, $\widetilde{Y}_{A_2}$, and filtered soot volume fraction, $\overline{f}_V$ on the spray center plane.

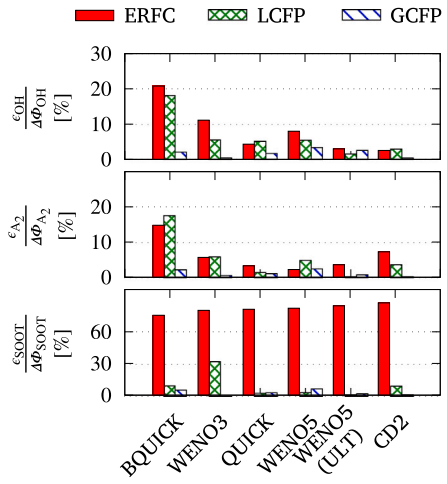

Fig. 3. Normalized scalar mass conservation errors for OH (top), naphthalene (center), and soot (bottom) for all three flow parameter models and scalar convection schemes.

injection LCFP case at 1 ms after Start-Of-Injection (SOI) was adopted as the initial solution. Note that all fuel has completely evaporated at this point, eliminating any mixture fraction or mass source terms in the test case and, thus, allowing the application of the GCFP model. To mitigate errors stemming from numerical integration in the GCFP model and discretization errors in the flamelet solver, the corresponding flamelet solution was interpolated to a finer grid comprising 383 points. Additionally, the time step size was reduced from approximately 100 to 10 ns to minimize numerical errors originating from time integration. The initial flow fields for the filtered mixture fraction, $\widetilde{Z}$, OH mass fraction, $\widetilde{Y}_{OH}$, naphthalene mass fraction, $\widetilde{Y}_{A_2}$, and soot volume fraction, $\overline{f}_V$ are shown in Fig. 2.

Six different numerical schemes have been employed for scalar convection, which feature different amounts of numerical dissipation and dispersion. Note that WENO5(ULT) refers to a WENO5 scheme with non-adaptive stencil weights that ensure higher numerical accuracy by sacrificing boundedness. Fig. 3 displays the scalar mass conservation error for OH, A_2, and soot over ten time steps, normalized by the total amount produced or consumed in that time period. Notably, the conventional model again exhibits poor conservation for soot, with up to 80 % mass lost due to inconsistent transport. This is expected due to the negligence of curvature effects in the ERFC model, which have been found to be crucial for soot transport in mixture fraction space [2]. Additionally, the conservation errors of the LCFP and, except for soot, the ERFC models are strongly influenced by the employed scalar scheme. In contrast, the GCFP model demonstrates consistently small errors.

Notably, the supposedly less accurate GCFP model exhibits superior conservation properties compared to the LCFP model, especially for the cases employing highly diffusive numerical schemes. The LCFP model provides accurate flow parameters for an instantaneous flow field, while the FDF evolution predicted by the LES flow solver is affected through numerical errors in the mixture fraction moment transport. The GCFP model incorporates these errors into the conditional flow parameters, thus, the errors cancel out when combining the flamelet solution with the FDF in Eq. (8). In other words, the GCFP model predicts the flow parameters consistently to the discretized FDF evolution, while the LCFP model is numerically more accurate but not discretely consistent.

Since the GCFP model shows good conservation properties for all scalar schemes, it can be used to approach the conservation issue from a different perspective, i.e., comparing the GCFP flow parameters with the LCFP predictions allows to quantify the effect of numerical errors from the scalar flow solver on the mixing process. Fig. 4 shows a comparison of the conditional flow parameters predicted at the initial time step. Note that just a single line is plotted for both the ERFC and the LCFP model since their prediction is scalar scheme independent. The top plot in Fig. 4 illustrates the global conditional dissipation rate, while the bottom plot represents the global mixture distribution function integrated over each flamelet grid cell. This bottom plot essentially depicts the total mass within a flamelet grid cell at a specific mixture fraction. Consistent with our previous findings [6], the ERFC and LCFP models exhibit similar predictions for conditional dissipation rates. As mentioned before, the GCFP model computes the flow parameters consistently with the discrete FDF evolution, and thus, the scalar dissipation rate of the GCFP model is strongly affected by the scalar convection scheme. Notable differences emerge at rich mixtures where $\widetilde{f}_G$ is small. These disparities may stem from numerical errors in the scalar convection scheme or, as discussed earlier, from the integration of the FDF in mixture fraction space. In some cases (WENO3, WENO5(ULT), and CD), negative values for χ_G are obtained, which are clipped to ensure flamelet solver stability. However, since $\widetilde{f}_G$ is very small in these cases, the impact on total scalar mass is marginal. In regions with substantially large $\widetilde{f}_G$, i.e., $\psi < 0.1$, the GCFP model appears to converge towards the LCFP model with more accurate schemes. The best agreement is found with the 2nd order central difference scheme (CD2), while WENO5(ULT) also shows good agreement. However, both schemes are prone to dispersive errors affecting the stability of the flow solver. It is interesting to note that among all scalar schemes used in this study, CD2 is the only one that discretely satisfies the product rule of differentiation, which is crucial in the derivation of the LCFP equations.

The global conditional diffusion rate is examined in the centered plot of Fig. 4. Notably, the ERFC model yields significantly different ξ_G predictions in terms of both shape and magnitude. The ERFC model predicts positive ξ_G for all mixtures with substantially large $\widetilde{f}_G$. Since ξ_G acts as a convection velocity for all soot scalars, it becomes clear that the ERFC model moves soot mass toward mixture zones of decaying probability, and thus, is inherently unable to conserve soot mass. On the other hand, the GCFP and LCFP models show similar ξ_G profiles, where again, the GCFP predictions tend to converge to the LCFP solution for scalar schemes of higher accuracy, while the best agreement is observed for the CD2 scalar scheme. However, it should be noted that the flow solver eventually becomes unstable when using the CD2 scheme.

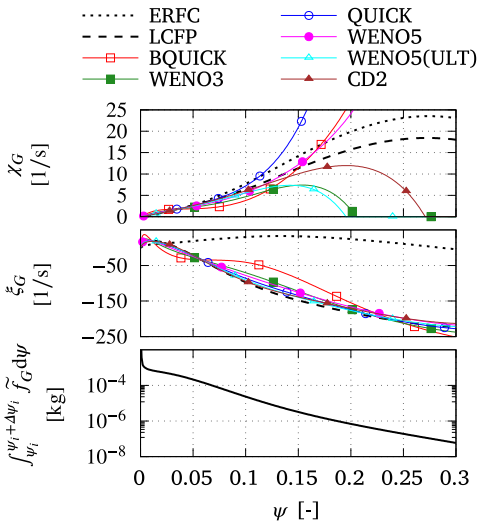

Fig. 4. Global conditional dissipation rate (top) and diffusion rate (center) predicted by the ERFC, LCFP, and GCFP models. The GCFP model is evaluated for several scalar convection schemes. The instantaneous mixture distribution is given in the bottom plot.

4. Summary and conclusion

The recently developed LCFP model [6] has been employed for the first time in a LES of spray combustion. The results have been compared to simulation results obtained using the conventional flow parameter model proposed by Peters [12]. As anticipated, the LCFP model exhibited enhanced scalar mass conservation properties compared to the conventional model, particularly concerning soot. Nevertheless, discernible conservation errors persist in the LCFP model. To determine the origin of these errors, a comparison was made between the LCFP model and the GFCP model [2]. This comparison was conducted in a simulation scenario configured to minimize numerical errors from time integration and discretization in mixture fraction space, using different scalar convection schemes. The GCFP model expresses the flow parameters consistently with the discretized FDF evolution and hence, demonstrated minimal scalar mass conservation errors. Notably, the LCFP model only achieved comparable mass conservation properties to the GFCP model when employing WENO5(ULT) or CD2. However, both schemes are prone to dispersion errors, which may impact the flow solver stability, emphasizing the need for further research concerning accurate and discretely consistent numerical scalar convection schemes.

Novelty and significance statement

Mixture fraction-based models decompose the transport of reactive scalars in physical space into scalar transport relative to mixture fraction and the transport of mixture fraction in physical space. While some approaches exist to consistently express these processes, there remains a noticeable gap in the literature regarding the impact of numerical errors on the modeled quantities. This paper addresses this critical gap by demonstrating that, in LES, numerical errors can significantly affect scalar mass conservation errors when employing non-premixed flamelet models. By elucidating the potential consequences of numerical errors, this work emphasizes the significance of employing accurate numerical methods. The findings presented herein not only contribute to the ongoing dialogue within the combustion science community but also underscore the importance of refining numerical approaches. This awareness is crucial for advancing the state-of-the-art in turbulent combustion modeling and, consequently, improving the efficiency and sustainability of technical devices.

CRediT authorship contribution statement

Marco Davidovic: Conceptualization, Methodology, Software, Validation, Formal analysis, Investigation, Resources, Data Curation, Writing – original draft. **Heinz Pitsch:** Conceptualization, Methodology, Resources, Writing – review & editing, Supervision, Project administration, Funding acquisition.

Declaration of competing interest

The authors declare that they have no known competing financial interests or personal relationships that could have appeared to influence the work reported in this paper.

Acknowledgments

This work was funded by the Deutsche Forschungsgemeinschaft (DFG, German Research Foundation) under Germany's Excellence Strategy – Exzellenzcluster 2186 "The Fuel Science Center" (ID: 390919832) and the German Federal Ministry of Education and Research (BMBF) and the Ministry for Culture and Science of the State of North Rhine-Westphalia (MKW) as part of the NHR funding.

The authors gratefully acknowledge the computing time provided to them by NHR4CES at RWTH Aachen University under the grant p0020437.

Appendix A. Supplementary data

Supplementary material related to this article can be found online at https://doi.org/10.1016/j.proci.2024.105537.

References

[1] K. Tsai, R.O. Fox, Modeling multiple reactive scalar mixing with the generalized IEM model, Phys. Fluids 7 (1995) 2820–2830.
[2] M. Davidovic, H. Pitsch, Formulation and importance of conservative transport in non-premixed flamelet models, Proc. Combust. Inst. 39 (2023) 2429–2438.
[3] S.B. Pope, Turbulent Flows, Cambridge University Press, 2000.
[4] R.O. Fox, Effect of the conditional scalar dissipation rate in the conditional moment closure, Phys. Fluids 32 (2020) 115118.
[5] A. Ilgun, A. Passalacqua, R. Fox, Application of quadrature-based moment methods to the conditional moment closure, Proc. Combust. Inst. 38 (2021) 2749–2757.
[6] M. Davidovic, H. Pitsch, Scalar mass conservation in turbulent mixture fraction based combustion models through consistent local flow parameters, Combust. Flame 262 (2024) 113329.
[7] S. Ghosal, An analysis of numerical errors in large-eddy simulations of turbulence, J. Comput. Phys. 125 (1996) 187–206.
[8] A. Kravchenko, P. Moin, On the effect of numerical errors in large eddy simulations of turbulent flows, J. Comput. Phys. 131 (1997) 310–322.
[9] F.K. Chow, P. Moin, A further study of numerical errors in large-eddy simulations, J. Comput. Phys. 184 (2003) 366–380.
[10] A. Triantafyllidis, E. Mastorakos, Implementation issues of the conditional moment closure model in large eddy simulations, Flow Turbul. Combust. 84 (2010) 481–512.
[11] H.-W. Ge, E. Gutheil, Probability density function (PDF) simulation of turbulent spray flows, At. Sprays 16 (2006) 531–542.
[12] N. Peters, Turbulent Combustion, Cambridge University Press, 2000.
[13] Y. Xuan, G. Blanquart, M.E. Mueller, Modeling curvature effects in diffusion flames using a laminar flamelet model, Combust. Flame 161 (2014) 1294–1309.
[14] M. Germano, U. Piomelli, P. Moin, W.H. Cabot, A dynamic subgrid-scale eddy viscosity model, Phys. Fluids A 3 (1991) 1760–1765.
[15] H. Kobayashi, The subgrid-scale models based on coherent structures for rotating homogeneous turbulence and turbulent channel flow, Phys. Fluids 17 (2005).
[16] R.S. Miller, J. Bellan, Direct numerical simulation of a confined three-dimensional gas mixing layer with one evaporating hydrocarbon-droplet-laden stream, J. Fluid Mech. 384 (1999) 293–338.
[17] M.A. Patterson, R.D. Reitz, Modeling the effects of fuel spray characteristics on diesel engine combustion and emission, SAE Trans. (1998) 27–43.
[18] H. Pitsch, E. Riesmeier, N. Peters, Unsteady flamelet modeling of soot formation in turbulent diffusion flames, Combust. Sci. Technol. 158 (2000) 389–406.
[19] A. Attili, F. Bisetti, M.E. Mueller, H. Pitsch, Effects of non-unity Lewis number of gas-phase species in turbulent nonpremixed sooting flames, Combust. Flame 166 (2016) 192–202.

[20] M. Davidovic, T. Falkenstein, M. Bode, L. Cai, S. Kang, J. Hinrichs, H. Pitsch, LES of n-dodecane spray combustion using a multiple representative interactive flamelets model, Oil Gas Sci. Technol. 72 (2017) 29.
[21] K. Narayanaswamy, G. Blanquart, H. Pitsch, A consistent chemical mechanism for oxidation of substituted aromatic species, Combust. Flame 157 (2010) 1879–1898.
[22] M. Mueller, G. Blanquart, H. Pitsch, Hybrid method of moments for modeling soot formation and growth, Combust. Flame 156 (2009) 1143–1155.
[23] O. Desjardins, G. Blanquart, G. Balarac, H. Pitsch, High order conservative finite difference scheme for variable density low mach number turbulent flows, J. Comput. Phys. 227 (2008) 7125–7159.
[24] B. Leonard, A stable and accurate convective modelling procedure based on quadratic upstream interpolation, Comput. Methods Appl. Mech. Engrg. 19 (1979) 59–98.
[25] M. Herrmann, G. Blanquart, V. Raman, Flux corrected finite volume scheme for preserving scalar boundedness in reacting large-eddy simulations, AIAA J. 44 (2006) 2879–2886.
[26] X.-D. Liu, S. Osher, T. Chan, Weighted essentially non-oscillatory schemes, J. Comput. Phys. 115 (1994) 200–212.
[27] F. Hu, M. Hussaini, J. Manthey, Low-dissipation and low-dispersion Runge–Kutta schemes for computational acoustics, J. Comput. Phys. 124 (1996) 177–191.
[28] D. Stanescu, W. Habashi, 2N-storage low dissipation and dispersion Runge–Kutta schemes for computational acoustics, J. Comput. Phys. 143 (1998) 674–681.
[29] A.C. Hindmarsh, P.N. Brown, K.E. Grant, et al., SUNDIALS: Suite of nonlinear and differential/algebraic equation solvers, ACM Trans. Math. Software 31 (2005) 363–396.